Title

Real-time dosimeter employed to evaluate the half-value layer in CT

Journal

Physics in Medicine and Biology, 59(2)

ISSN

0031-9155

Authors

McKenney, Sarah E
Seibert, J Anthony
Burkett, George W
et al.

Publication Date

2014-01-20

DOI

10.1088/0031-9155/59/2/363

Peer reviewed

HHS Public Access

Author manuscript

Phys Med Biol. Author manuscript; available in PMC 2015 March 23.

Published in final edited form as:

Phys Med Biol. 2014 January 20; 59(2): 363–377. doi:10.1088/0031-9155/59/2/363.

Real-time dosimeter employed to evaluate the half-value layer in CT

Sarah E. McKenney[1,2], **J. Anthony Seibert**[1,2], **George W. Burkett**[1], **Dale Gelskey**[3], **Paul B. Sunde**[4], **James D. Newman**[2], and **John M. Boone**[1,2]

John M. Boone: jmboone@ucdavis.edu

[1]Department of Biomedical Engineering Graduate Group, University of California Davis, Davis, California

[2]Department of Radiology, University of California Davis Medical Center, Sacramento, California

[3]Diagnostic Imaging Specialists Corporation, Toronto, Canada

[4]Radcal, Monrovia, California

Abstract

Half-value layer (HVL) measurements on commercial whole body CT scanners require serial measurements and, in many institutions, the presence of a service engineer. An assembly of aluminum filters (AAF), designed to be used in conjunction with a real-time dosimeter, was developed to provide estimates of the HVL using clinical protocols. Two real-time dose probes, a solid-state and air ionization chamber, were examined. The AAF consisted of eight rectangular filters of high purity aluminum (Type 1100), symmetrically positioned to form a cylindrical "cage" around the probe's detective volume. The incident x-ray beam was attenuated by varying thicknesses of aluminum filters as the gantry completed a minimum of one rotation. Measurements employing real-time chambers were conducted both in service mode and with a routine abdomen/pelvis protocol for several combinations of x-ray tube potentials and bow tie filters. These measurements were validated against conventional serial HVL measurements. The average relative difference between the HVL measurements using the two methods was less than 5% when using a 122 mm diameter AAF; relative differences were reduced to 1.1% when the diameter was increased to 505 mm, possibly due to a reduced scatter contamination. Use of a real-time dose probe and the AAF allowed for time-efficient measurements of beam quality on a clinical CT scanner using clinical protocols.

Keywords

CT; real-time dosimetry; beam quality; half-value layer

1. Introduction

Extensive work has shown that transmission measurements, such as those used to calculate the half value layer (HVL), adequately characterize the absorption properties of a diagnostic x-ray beam (Bell, 1936; Boone, 1986; Delgado and Ortiz, 1997; Greening, 1963; Kaye, 1934; Poirier *et al.*; Ruth and Joseph, 1997; Silberstein, 1932).

Conventionally, the HVL is estimated using a serial method with aluminum filters of different thicknesses where a separate x-ray exposure is required for each filter while the source remains stationary (Hill, 1999). Despite the fact that HVL is annually assessed for mammography units (FDA, 2002) and most other x-ray systems to evaluate output constancy, the HVL is not required to be regularly assessed on CT systems (Kruger *et al.*, 2000). In many institutions, a service engineer is required in order to stop gantry rotation for a serial, stationary-source measurement procedure.

While there is no definitive method for measuring the HVL of a CT scanner as the source is rotating, several methods have been proposed (Kruger *et al.*, 2000; Maia and Caldas, 2006). The advantage of these methods is that the HVL is evaluated with an integrating ionization chamber as the source rotates. However, these approaches still employ a serial method where rings of aluminum filters are sequentially added between a series of axial CT exposures.

Real-time x-ray dosimeters have made significant advancements in recent years (Hyer *et al.*, 2009) and are becoming commercially available. These dosimeters not only resolve temporal changes in radiation flux, but they also provide an opportunity to reinvent standard quality control protocols. In this investigation, the aims are to demonstrate the feasibility of characterizing x-ray beam quality using a real-time dose probe and a prototype assembly of aluminum filters (AAF). This new approach for HVL measurement in CT capitalizes on the x-ray source rotation, and in doing so, eliminates the need for serial measurements using different filter thicknesses.

2. Methods

The AAF was fabricated using aluminum filters of varying thicknesses positioned symmetrically around the real-time dose probe (see figure 1). As the x-ray source rotated around the apparatus, the x-ray beam was intercepted and attenuated by a number of filters with different thicknesses. While a standard ion chamber would simply integrate the air kerma from the entire acquisition, the real-time dose probe resolves the air kerma rate of the incident beam throughout the gantry rotation sequence. Exploiting the spaces between the plates for measurements of the unattenuated beam, relative transmission measurements were made and used to estimate the HVL.

2.1 Materials: HVL assembly of aluminum filters (AAF)

Eight aluminum filters with different thicknesses were assembled onto an apparatus, which will be referred as an Assembly of Aluminum Filters (AAF). Plates of high-purity (Type 1100) aluminum were manufactured in an assortment of thicknesses such that they could be combined to characterize the HVL for spectra over a wide range of beam qualities. The filter thicknesses ranged from 0.81 mm to 9.52 mm and all filters had a width of 25 mm and a length of 102 mm. The modular nature of the filters allowed them to be easily exchanged and combined, resulting in a large number of possible filter thicknesses. Total filter thicknesses were selected to be above and below the estimated HVL of a scanner, providing a robust dataset for interpolation of the HVL.

Two AAF's were constructed for this work. The small diameter AAF (AAF_{small}) consisted of two octagonal endplates, constructed from aluminum, that were used to support the high-purity aluminum filters (see figure 2). The center position of the inner face of each filter was positioned at a radius of 61 mm from the central axis of the apparatus. There was a gap of 24 mm between each of the filters approximating the width of each filter. The ends of the filters were fixed to the flat sides of the octagonal frame.

To reduce the impact of x-ray scatter in the measurement, a 505 mm diameter AAF (AAF_{large}) was constructed by replacing the end caps with foam board. The foam board had a thickness of 5 mm and supported the aluminum filters with a small L-bracket at one edge (see figure 3). To reduce angle-dependent bias in the measurements as the x-ray tube rotated around the assembly, the filter thickness was alternated for both AAF's. Extension rods were attached to each apparatus to allow centering within the CT beam.

2.2 Materials: Real-time dose probes

Two real-time dose probes were used in this investigation. One probe had a solid-state detector while the other was an air ionization chamber. Both dose probes were used for relative transmission measurements associated with the AAF. Conventional HVL measurements were conducted with a 0.6 cm^3 thimble chamber and an integrating electrometer (Accu-Pro, Radcal, Monrovia, CA).

2.2.1 The real-time solid-state dosimeter—The real-time solid-state (RTSS) dosimeter was a prototype real-time chamber (Diagnostic Imaging Specialists Corporation (DISC), St. Malo, Canada). The active volume of the probe was a cylinder with a diameter of 5 mm and a length of 7 mm. The acquisition software allowed the sampling rate to be switched between 100 Hz and 1000 Hz. The output signal was digitized in parallel using four channels, corresponding to four different gains (×1, ×10, ×100, or ×1000), which extended the dynamic range of the device. The nonlinear energy response of the solid-state detector was corrected as described in Appendix A.

2.2.2 The real-time air ionization chamber—The real-time air ionization (RTAI) chamber was a 0.6 cm^3 thimble chamber coupled to a real-time electrometer (Accu-Gold, Radcal, Monrovia, CA). The output of the electrometer was recorded by a laptop computer using a USB-2 interface. This chamber had an active volume that was 18.7 mm in length and 9.5 mm in diameter. The sampling rate was 10 kHz and measurements were acquired using manufacturer-provided software.

The angular response of the RTAI chamber was assessed on a dedicated breast CT (bCT) scanner (Boone *et al.*, 2006). The rotational isotropy of the RTSS chamber was previously reported (McKenney *et al.*, 2011) to have a relative angular measurement uncertainty of 0.80%. For the RTAI chamber, measurements were also made with a stationary source. A beam with a tube potential of 120 kV and tube current of 8 mA was filtered with 0.2 mm of copper. The probe was held fixed at system isocenter. The probe was manually rotated in $\frac{\pi}{2}$ increments; a 5-second exposure was made at each angular position. A total of four

measurements were made at each angular position; all air kerma measurements were then normalized to the average of the four positions.

The results of the isotropy measurements are presented in figure 4. The relative angular measurements had an average measurement uncertainty of 0.5%. The primary contribution to the measurement uncertainty was the effect of manually rotating the probe. Because the anisotropy was relatively minor and the average difference was reasonably low, the angular response of the RTAI chamber was assumed to be uniform.

2.3 System setup: Clinical CT scanner

The two AAF configurations were used in a clinical CT setting to assess their utility for HVL assessment. All measurements were made on a LightSpeed VCT scanner (General Electric, Waukesha, WI). The scanner had a source to isocenter distance of 541 mm and a scan field of view (SFOV) of 500 mm. The patient table was retracted from the field of view for all measurements.

2.4.1 Methods: Conventional HVL method (stationary source) in service mode—Conventional HVL measurements were first made with each of the eight aluminum filters using a 0.6 cm^3 dose accumulation mode chamber (Accu-Pro, Radcal, Monrovia, CA) (see figure 5). The integrating chamber was placed at the scanner's isocenter by fixing it to an extension rod. With the CT scanner in service mode, the x-ray source was positioned at the bottom of the gantry (6 o'clock position) and was held stationary. Aluminum filters of differing thicknesses were placed on the gantry cowling between each x-ray exposure. The filter thicknesses ranged from 0.8 to 15.8 mm. An exposure time of one second was used. To reduce scatter contamination in the measurement, the beam was collimated to 5 mm (at isocenter). A measurement uncertainty of <2% (k=2) was assumed. This method was repeated at 80 kV, 100 kV, 120 kV and 140 kV with a medium bow tie filter. The HVL was also measured with the bow tie filters retracted (i.e. air), and with the small, medium, and large bow tie filter at 120 kV. Using the eight filters from the AAF, eight measurements were made for each combination of tube potential and bow tie filter. For all measurements, the small focal spot and a tube current of 200 mA was used.

2.4.2 Methods: AAF_{small} (rotating source) in service mode—To ensure consistency in technique factors for each combination of filter and tube potential, the AAF configuration was first validated against conventional HVL measurements while using the scanner in service mode. The same aluminum filters that were used for the conventional serial HVL measurements were mounted onto the AAF_{small}. The extension rods of the apparatus were attached to an external support so that there were no additional attenuating or scattering materials in the field of view. The set-up was centered at the scanner's laser-indicated isocenter (see figure 6). The time for one gantry rotation was set to 1 s in axial mode.

Because of differences in the sensitivity and dynamic range of the two probes, the tube current was set to 10 mA for the RTSS probe and 400 mA for the RTAI chamber. Rotating source measurements were made for all combinations of x-ray tube potentials and bow tie filters using each real-time dose probe separately. Partial probe exposure could amplify any

angular effects of slightly mispositioning the probe off of isocenter. To fully irradiate the probes, the beam was collimated to the length of the radiation meters' sensitive volume. Measurements made with the RTSS probe used a beam width of 10 mm while measurements made with the RTAI chamber used a beam width of 20 mm.

2.5 Methods: AAF_{large} (rotating source) in clinical mode

HVL measurements were repeated for a series of tube potentials in clinical mode using a standard abdomen/pelvis protocol. A rotation time of 1 second was used and the tube current was manually set to 400 mA, with no tube current modulation. Because of increased scatter detected by the AAF_{small}, the AAF_{large} was used instead. Additionally, the range of filter thicknesses was reduced to improve sampling around the estimated HVL; filter thicknesses ranged from 4.8 to 10.3 mm. Beam widths of both 20 mm and 40 mm were also examined with the RTAI chamber.

2.6.1 Analysis: Signal corrections—Due to imprecision in centering the AAF, the effects of the inverse square law (ISL) were apparent in the unattenuated portions of the measured signal train (Fig. 7.a). The periodic nature of the signal was a result of using a helical acquisition mode; the ISL appeared as a low-frequency sinusoidal modulation present in the signal train with the same period as the gantry rotation. The different aluminum filters attenuated the incident beam and are seen as a high frequency component of the signal train. For this acquisition, a 1 second rotation time was used for a 4 second total exposure time at 120 kV and 400 mA with a large bow tie filter. Multiple gantry rotations allow for a greater number of samples for each beam filter. A previously-described correction algorithm (McKenney *et al.*, 2011) was used to reduce the effects of the inverse square law, which analyzed the unattenuated portions of the signal train and applied a sinusoidal scaling correction to the entire dataset (Fig 7.b).

For each filter thickness, the relative transmission was computed as the average value of the filtered signal to the average value of the unattenuated signal. The HVL was estimated using a second-order polynomial fit to the log of the eight relative transmission measurements.

2.6.2 Analysis: Statistics—The relative difference between HVLs measured with the AAF configuration and the conventional method was evaluated as

$$\text{relative difference} = \frac{|HVL_{rotating\ source} - HVL_{conventional}|}{HVL_{conventional}}. \quad \text{(Eq. 1)}$$

3. Results

3.2 HVL measurements in service mode

A summary of the measurements performed on the whole body CT scanner is shown in Table 1. The raw signal of an HVL measurement using a standard rotating gantry acquisition, the RTAI probe, and AAF_{small} is plotted in figure 7. In this figure, the probe was estimated to be 7.5 mm from rotational isocenter. Without the ISL correction, the HVL was measured as 7.82 mm Al; with the correction, it reduced to 7.76 mm Al.

Across the four tube potentials (figure 8), the average relative difference of the HVL measured with the AAF_{small} was 1.9% with the RTSS probe and 3.9% with the RTAI chamber, compared to the conventional, stationary-source method. When evaluated across the different bow tie filters (figure 9), the average relative difference was 2.1% with the RTSS probe and 4.6% with the RTAI chamber. The HVL measurements made with conventional techniques and with the AAF_{small} method were significantly different when using a two-tailed, paired t-test ($p > 0.001$).

3.3 HVL measurements in clinical mode

Acquisitions performed with the AAF_{large} had similar general features to t the AAF_{small} results depicted in Fig. 7.b, but with narrower attenuation time intervals (figure 10) because the width of the aluminum filters was held constant. While the value of the unattenuated air kerma rate is comparable between the two plots, the range of attenuated values differed because a more limited range of filter thicknesses was used in the AAF_{large} configuration.

A slightly negative bias was observed in the correlation of the HVL measurements across the four tube potentials with the 20 mm collimation (figure 11); an average relative difference of 0.2% was estimated. A positive bias, with an average relative difference of 0.8%, was observed for the 40 mm beam width.

The average relative difference across the three bow tie filters was 0.6% for the 20 mm beam collimation, which increased to 1.6% for a beam width of 40 mm (figure 12). The conventional HVL measurement and the AAF_{large} measurement (with a 20 mm beam collimation) were not found to be significantly different when using a two-tailed, paired t-test ($p>0.5$).

4. Discussion

The results of HVL measurements with the AAF configuration and a real-time dosimeter demonstrate the feasibility of conducting HVL measurements from a minimum of one single CT scan. Semi-automated software developed in our laboratory corrects the signal and calculates the HVL in approximately 2 seconds. The AAF method makes routine assessment of CT beam quality more feasible. The HVL data can be used for routine consistency testing. For CT dosimetry research the HVL may be used to model the x-ray spectra in Monte Carlo simulations (Ay *et al.*, 2005; Bazalova and Verhaegen, 2007; Bhat *et al.*, 1998; Birch and Marshall, 1979; Boone, 1986; Turner *et al.*, 2009). It should be noted that the HVL does not uniquely characterize a spectrum (Baird, 1981). The use of the AAF_{large} with rotating gantry protocols enables the investigator to characterize HVL's across a complete range of tube potentials and bow tie filters within the time constraints of the CT scanner's availability.

With the AAF_{small}, a systematic overestimate of the HVL was observed, which is attributed to scatter contamination in this geometry. Even with this observed bias, an average relative difference in the HVL assessment of only 4.1% was measured. Increasing the diameter of the AAF reduced the HVL measurement's relative difference to 1.1%, even when using a more scatter prone large beam collimation width. It is possible that the conventional HVL

measurements contain a small bias as the International Atomic Energy Agency (IAEA) recommends a second set of collimators between the filter and detector (IAEA, 2007), not included in set-up for the conventional measurements of this investigation.

There was a notable increase in the relative difference of the RTSS probe's measurement of the HVL of the large bow tie filter. The technical specification document for the CT scanner (G.E. Healthcare, 2010) states that the large bow tie filter has an additional 0.075 mm of copper; it is likely that the assumption of an aluminum-only inherent filtration material in the energy correction algorithm led to some inaccuracy in the HVL measurement. Solid-state probes on the market may also exhibit this fallibility. The HVL can be accurately measured with these devices from a single exposure if the electrometer software appropriately corrects for beam quality. The HVL of composite filters, such as the large bow tie filter, cannot be accurately estimated unless the amounts of each material are known, in a sense, defeating the purpose of an HVL measurement.

It is difficult to differentiate the small and medium bow tie filters using solely the HVL measurement on the CT scanner evaluated because there is a <1% difference between the two HVL values. The AAF configuration specifically characterizes x-ray beam quality at the center of the field of view. For a more complete description of the x-ray output of the scanner, it is necessary to evaluate the angularly-dependent air kerma profile. By employing the *characterization of bow tie filter relative attenuation* (COBRA) method (Boone, 2009; McKenney *et al.*, 2011) in conjunction with the AAF HVL measurement, a complete assessment of the small bow tie filter from the medium filter can be made. The COBRA method requires the inherent filtration of the system, which was determined from an HVL measurement at isocenter.

Scatter contamination was found to play a noticeable role in the HVL measurements. Ideally, the x-ray beam's width should be collimated as tightly as possible to the dosimeter as observed previously (Delgado and Ortiz, 1997). Maximizing the AAF diameter by fixing plates to the gantry reduces scatter and eliminates the need for an external fixture. This is a more invasive experimental design and it requires either larger aluminum filters or a slower rotation time for the real-time probe to temporally resolve the attenuated portions of the beam.

The AAF can be used with any real-time dose probe; however, there are several important considerations. First, the probe must have high temporal resolution so that multiple measurements can be made on each filter, and that these can be distinguished from air. While the RTSS probe had a sampling rate of 1 kHz, slower sampling rates are acceptable, particularly with slower gantry rotation speeds. Secondly, the real-time probe must have a dynamic range that is matched to the output range of the CT system. Finally, an energy response correction scheme for solid-state probes is necessary for accurate relative transmission measurements in air.

When collecting HVL measurements, a number of samples should be acquired to ensure a reasonable estimate of the attenuation values. This can be achieved by increasing the number of gantry rotations collected during an acquisition, either by increasing the rotation

speed or by increasing the exposure time. For reliable HVL measurements the dosimeter must be placed at a consistent z-position in the field to mitigate the spectral shifts from the heel effect (Ay *et al.*, 2004). An external fixture to support the AAF from the back of the gantry, allowed for measurements to be acquired in helical mode (in which the table moves outside of the FOV). It is also possible to measure the HVL by suspending the AAF off edge of the patient table while using axial or cine scan mode, providing that the table remains stationary during the acquisition. The set-up requirements are relatively minimal and the device is more easily transportable in the latter configuration. The downside of measurements conducted in an axial mode, is that the start-stop angle sometimes obscures the attenuation profile of one of the filters. With either acquisition mode, it is essential to deactivate tube current modulation for correct relative transmission measurements.

5. Conclusions

Using a real-time dose probe and an assembly of aluminum filters, the HVL can be measured on a clinical CT scanner. HVL measurements were evaluated with both a real-time air ionization chamber and an energy-corrected real-time solid-state probe. With access to a real-time dose probe and the AAF it is possible to monitor the beam quality of a clinical CT scanner easily, accurately, and without the need to enter the service mode of the scanner. HVL measurements made at the central ray in conjunction with the characterization of bow tie relative attention provide a more complete description of the x-ray output of a CT scanner. These measurement techniques can be used for both routine quality assessment measurements or for spectral estimation for Monte Carlo simulations.

Acknowledgements

This research was funded in part by a grant from the NIH (R01 EB002138), the University of California, Davis Professional Liability Rebate program's Loss Prevention grant, and a grant from the Office of the President of the University of California system. The authors would like to thank Dr. Kai Yang, Dr. Shin-ying Huang, and Dr. Alex Kwan for their invaluable assistance.

Appendix A

Energy response correction algorithm for a solid-state detector

Custom software was developed to convert the relative transmission measurements of the RTSS probe into relative measurements of an ideal ion chamber for a known x-ray tube potential. The method was deemed appropriate for the purposes of this work with an average percent difference of 2.3% between the HVL measurements made with the RTSS probe and a general purpose ion chamber (10X5-6 ion chamber and 9010 radiation monitor, Radcal, Monrovia).

The mean energy imparted to the solid-state probe $\varepsilon_{RTSS}(x)$ was modeled by

$$\varepsilon_{RTSS}\left(x_{filter}\right) = A\int_{E_{min}}^{E_{max}} E\Phi_E e^{-\mu_{Al}(E)x_{inherent}} e^{-\mu_{Al}(E)x_{filter}} \left(1 - e^{-\mu_{probe}(E)x_{probe}}\right) dE, \quad \text{(Eq. A.1)}$$

where E was the photon energy and x was a material's thickness. The photon distribution of photon fluence with respect to energy Φ_E [mm^{-2} keV^{-1}] at the detector position for an

unattenuated beam was simulated using the TASMIP spectral model (Boone and Seibert, 1997). The energy dependent linear attenuation coefficient μ(*E*) was determined from a tabulated dataset (Boone and Chavez, 1996). The probe's manufacturer provided the material composition of the real-time probe's active volume. The thickness of the detector was also proprietary information and was determined from tomographic images of the active volume of the probe. The cross-sectional area of the active volume *A*, was unknown as it canceled in the relative transmission measurement (Eq. A.2). The aluminum filters' thicknesses, x_{filter}, were known. While the inherent filtration thickness $x_{inherent}$ of the beam was unknown, the inherent filter was assumed to be composed of aluminum.

The relative transmission *R* for both empirical (R_{emp}) and simulated (R_{sim}) measurements was determined by

$$R\left(x_{filter}\right)=\frac{\varepsilon_{RTSS}\left(x_{filter}\right)}{\varepsilon_{RTSS}\left(x_{filter}=0\right)}. \quad \text{(Eq. A.2)}$$

Using a least-squares algorithm, the optimal inherent filter thickness was determined by iterating over increasing inherent filter thicknesses and identifying the $x_{inherent}$ that minimized χ^2,

$$\arg\min_{x_{inherent}}\chi^2,\ \chi^2=\sum_{x_{filter}=x_1}^{x_{filter}=x_N}\left[R_{emp}\left(x_{filter}\right)-R_{sim}\left(x_{filter},x_{inherent}\right)\right]^2. \quad \text{(Eq. A.3)}$$

The energy corrected relative transmission was then determined by simulating the collision air kerma, K_c, measured with an ideal ion chamber. Using the optimal inherent filter thickness $x_{inherent,optimal}$, the collision kerma measurement was modeled as

$$K_c\left(x_{filter}\right)=\int_{E=0}^{E_{max}}\left[\frac{\mu_{abs}(E)}{\rho}\right]_{air}E\Phi_E e^{-\mu_{Al}(E)x_{inherent,optimal}}e^{-\mu_{Al}(E)x_{filter}}dE. \quad \text{(Eq. A.4)}$$

Where $\left[\frac{\mu_{abs}(E)}{\rho}\right]_{air}$ was the mass energy absorption in air, also determined from a tabulated dataset (Boone and Chavez, 1996). Other quantities have the same meaning as in Eq. A.1. With minor adjustments to Eq. A.4, exposure and air kerma could be modeled instead. Because the relative transmission of collision air kerma, air kerma and exposure are approximately equal in diagnostic energy ranges (ICRU, 2011), the relative transmission calculated would be approximately equivalent. The energy corrected HVL was then determined from the relative transmission simulated in air (see section 2.6.1).

References

Ay MR, Sarkar S, Shahriari M, Sardari D, Zaidi H. Assessment of different computational models for generation of x-ray spectra in diagnostic radiology and mammography. Medical Physics. 2005; 32:1660–1675. [PubMed: 16013725]

Ay MR, Shahriari M, Sarkar S, Adib M, Zaidi H. Monte Carlo simulation of x-ray spectra in diagnostic radiology and mammography using MCNP4C. Physics in Medicine and Biology. 2004; 49:4897–4917. [PubMed: 15584526]

Baird LC. X-ray spectra vs attenuation data: A theroretical analysis. Medical Physics. 1981; 8:319–323. [PubMed: 7322056]

Bazalova M, Verhaegen F. Monte Carlo simulation of a computed tomography x-ray tube. Physics in Medicine and Biology. 2007; 52:5945–5955. [PubMed: 17881811]

Bell GE. Spectral distribution in continuous X-ray spectrum and specification of X-ray quality. British Journal of Radiology. 1936; 9:680–688.

Bhat M, Pattison J, Bibbo G, Caon M. Diagnostic x-ray spectra: A comparison of spectra generated by different computational methods with a measured spectrum. Medical Physics. 1998; 25:114–120. [PubMed: 9472833]

Birch R, Marshall M. Computation of bremsstrahlung x-ray spectra and comparison with spectra measured with a Ge(Li) detector. Physics in Medicine and Biology. 1979; 24:505–517. [PubMed: 461510]

Boone JM. Equivalent spectra as a measure of beam quality. Medical Physics. 1986; 13:861–868. [PubMed: 3796483]

Boone JM. Method for evaluating bow tie filter angle-dependent attenuation in CT: Theory and simulation results. Medical Physics. 2009; 37:40–48. [PubMed: 20175464]

Boone JM, Chavez AE. Comparison of x-ray cross sections for diagnostic and therapeutic medical physics. Medical Physics. 1996; 23:1997–2005. [PubMed: 8994164]

Boone JM, Nelson TR, Kwan ALC, Yang K. Computed tomography of the breast: Design, fabrication, characterization, and initial clinical testing. Medical Physics. 2006; 33:2185.

Boone JM, Seibert JA. Accurate method for computer-generating tungsten anode x-ray spectra from 30 to 140 kV. Medical Physics. 1997; 24:1661–1670. [PubMed: 9394272]

Delgado V, Ortiz P. Determination of the energy fluence of diagnostic X-ray beams from field measurements of attenuation curves. Medical Physics. 1997; 24:1089–1095. [PubMed: 9243471]

FDA. Mammography Quality Standards; Final Rule. In: H a H Services. , editor. 900.12(e) Quality Control. 2002.

G E Healthcare General Electric Company. , editor. G.E. Healthcare. LightSpeed VCT: Technical Reference Manual, English. 2010.

Greening JR. The Derivation of Approximate X-ray Spectral distributions and an Analysis of X-ray 'Quality' Specifications. British Journal of Radiology. 1963; 36:363–371. [PubMed: 13950192]

Hill AL. Half value layer measurements to facilitate patient dose assessment for newer CT scanners using published normalized dose data. British Journal of Radiology. 1999; 72:792–798. [PubMed: 10624346]

Hyer DE, Fisher RF, Hintenlang DE. Characterization of a water-equivalent fiber-optic coupled dosimeter for use in diagnostic radiology. Medical Physics. 2009; 36:1711–1716. [PubMed: 19544788]

IAEA. Technical Report Series 457. Vienna: IAEA; 2007. Dosimetry in diagnostic radiology: An international code of practice.

ICRU. Fundamental quantities and units for ionizing radiation (*revised*). In: Seltzer, SM., editor. Report No. 85a. Oxford: Oxford University Press; 2011.

Kaye GWC. X rays. Reports on Progress in Physics. 1934; 1:228.

Kruger RL, McCollough CH, Zink FE. Measurement of half-value layer in x-ray CT: A comparison of two noninvasive techniques. Medical Physics. 2000; 27:1915–1919. [PubMed: 10984237]

Maia AF, Caldas LVE. A simple method for evaluation of half-value layer variation in CT equipment. Physics in Medicine and Biology. 2006; 51:1595–1601. [PubMed: 16510965]

McKenney SE, Nosratieh A, Gelskey D, Yang K, Huang S-y, Chen L, Boone JM. Experimental validation of a method characterizing bow tie filters in CT scanners using a real-time dose probe. Medical Physics. 2011; 38:1406–1415. [PubMed: 21520852]

Poirier Y, Kouznetsov A, Tambasco M. A simplified approach to characterizing a kilovoltage source spectrum for accurate dose computation. Medical Physics. 2012; 39:3041–3050. [PubMed: 22755689]

Ruth C, Joseph PM. Estimation of a photon energy spectrum for a computed tomography scanner. Medical Physics. 1997; 24:695–702. [PubMed: 9167160]

Silberstein L. Determination of the spectral composition of x-ray radiation from filtration data. Journal of the Optical Society of America. 1932; 22:265–280.

Turner AC, Zhang D, Kim HJ, DeMarco JJ, Cagnon CH, Angel E, Cody DD, Stevens DM, Primak AN, McCollough CH, McNitt-Gray MF. A method to generate equivalent energy spectra and filtration models based on measurement for multidetector CT Monte Carlo dosimetry simulations. Medical Physics. 2009; 36:2154–2164. [PubMed: 19610304]

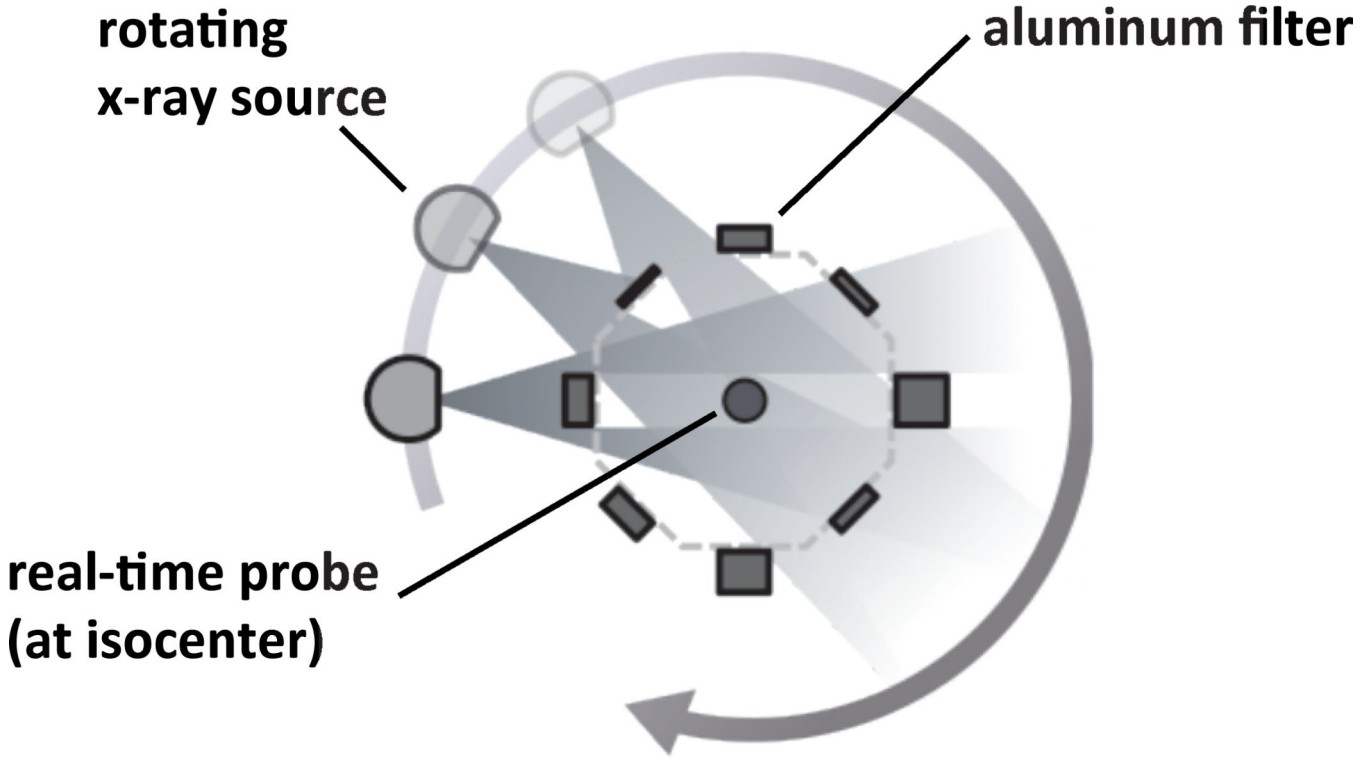

Figure 1.
Diagram of the HVL apparatus of aluminum filters (AAF). The aluminum filters, supported by octagonal end caps, attenuate the x-ray beam by varying amounts, while the gaps between the filters provide the projected unfiltered x-ray beam required for comparison.

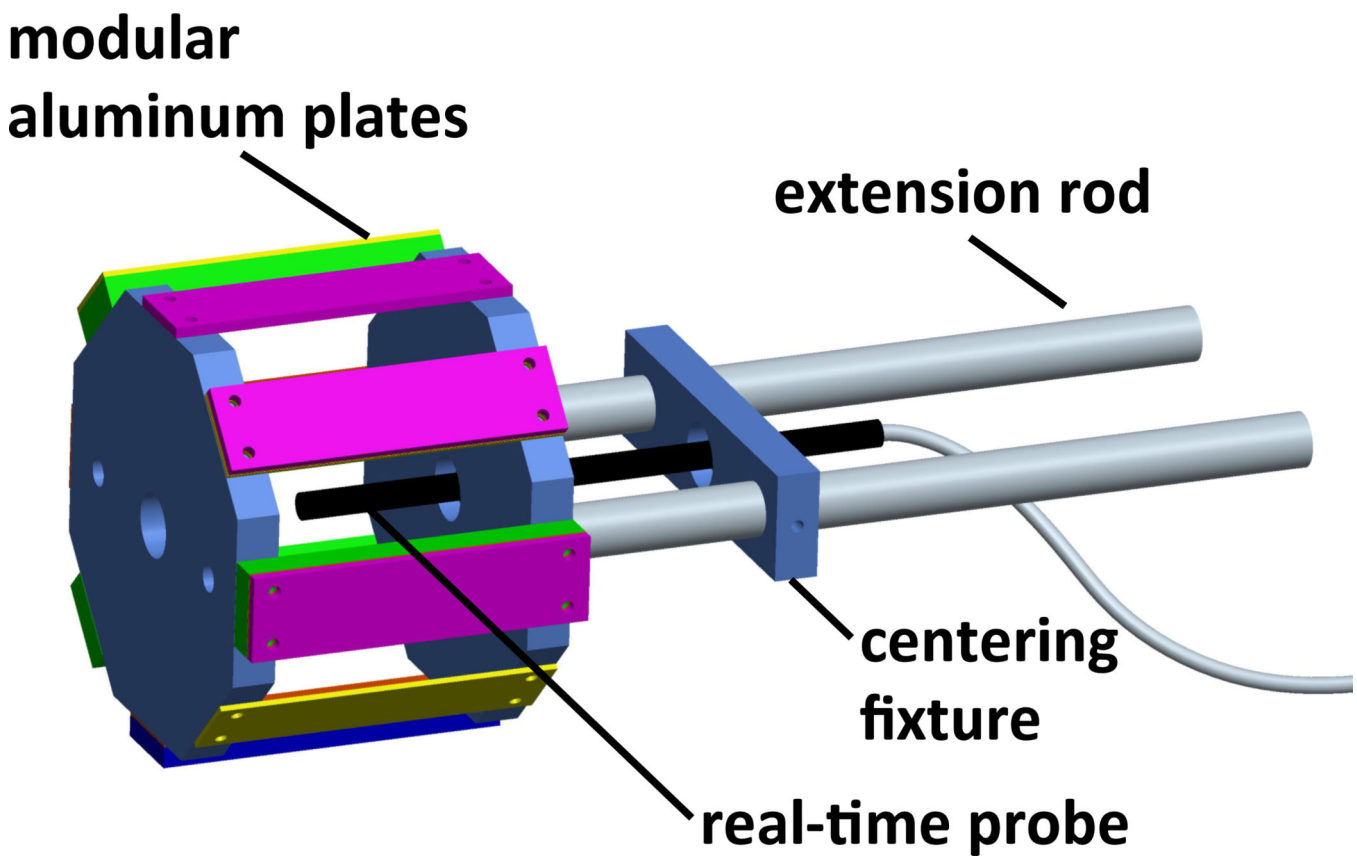

Figure 2.
Diagram of small diameter apparatus of aluminum filters (AAF_{small}), with a diameter of 122 mm, and the real-time solid state (RTSS) probe centered within it.

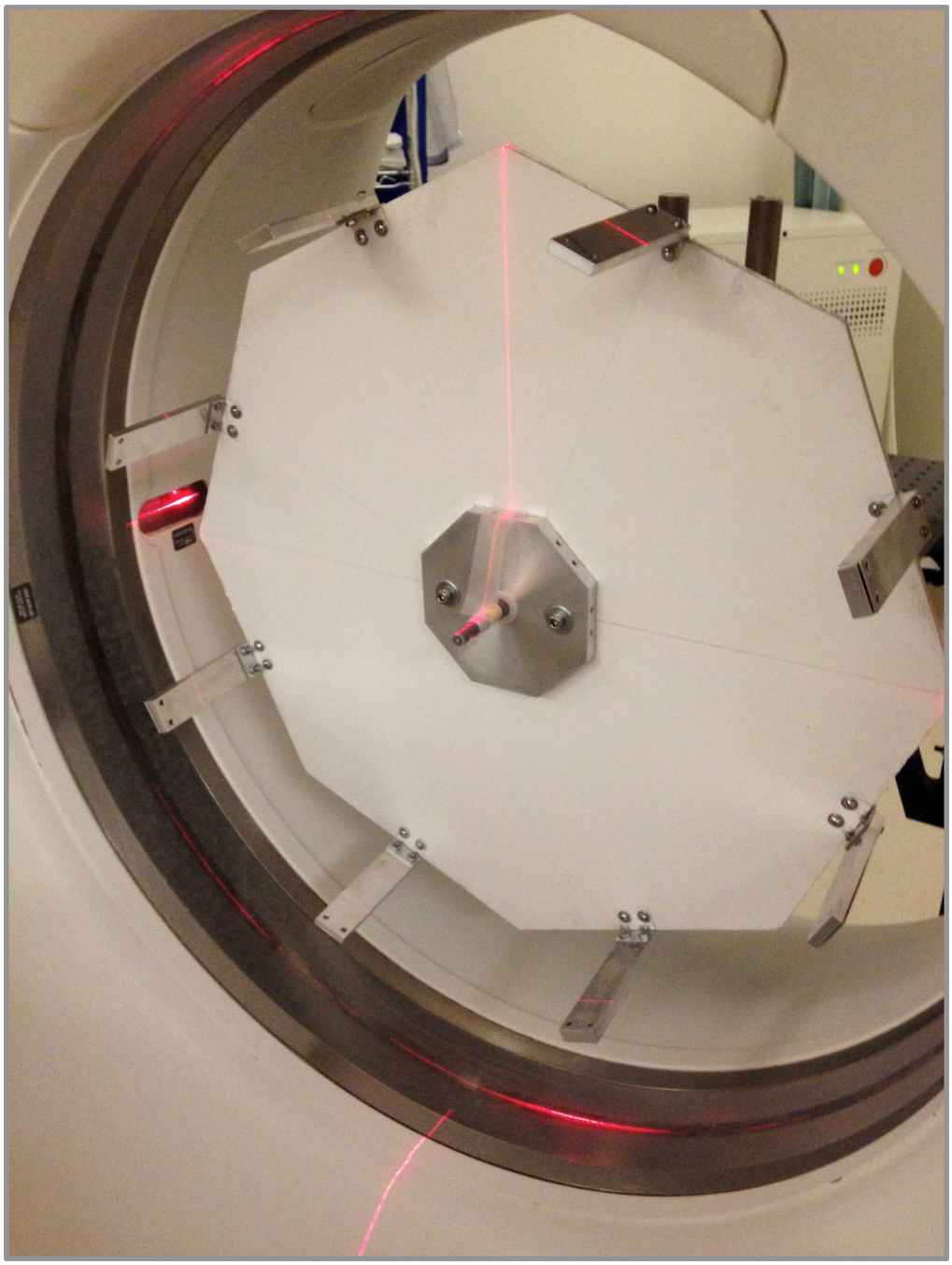

Figure 3.

Photograph of the large diameter apparatus of aluminum filters (AAF_{large}), with a diameter of 505 mm. The configuration had an open face with each aluminum filter attached to an edge of the foam board. The 0.6 cm^3 real-time air ionization (RTAI) chamber was positioned at isocenter.

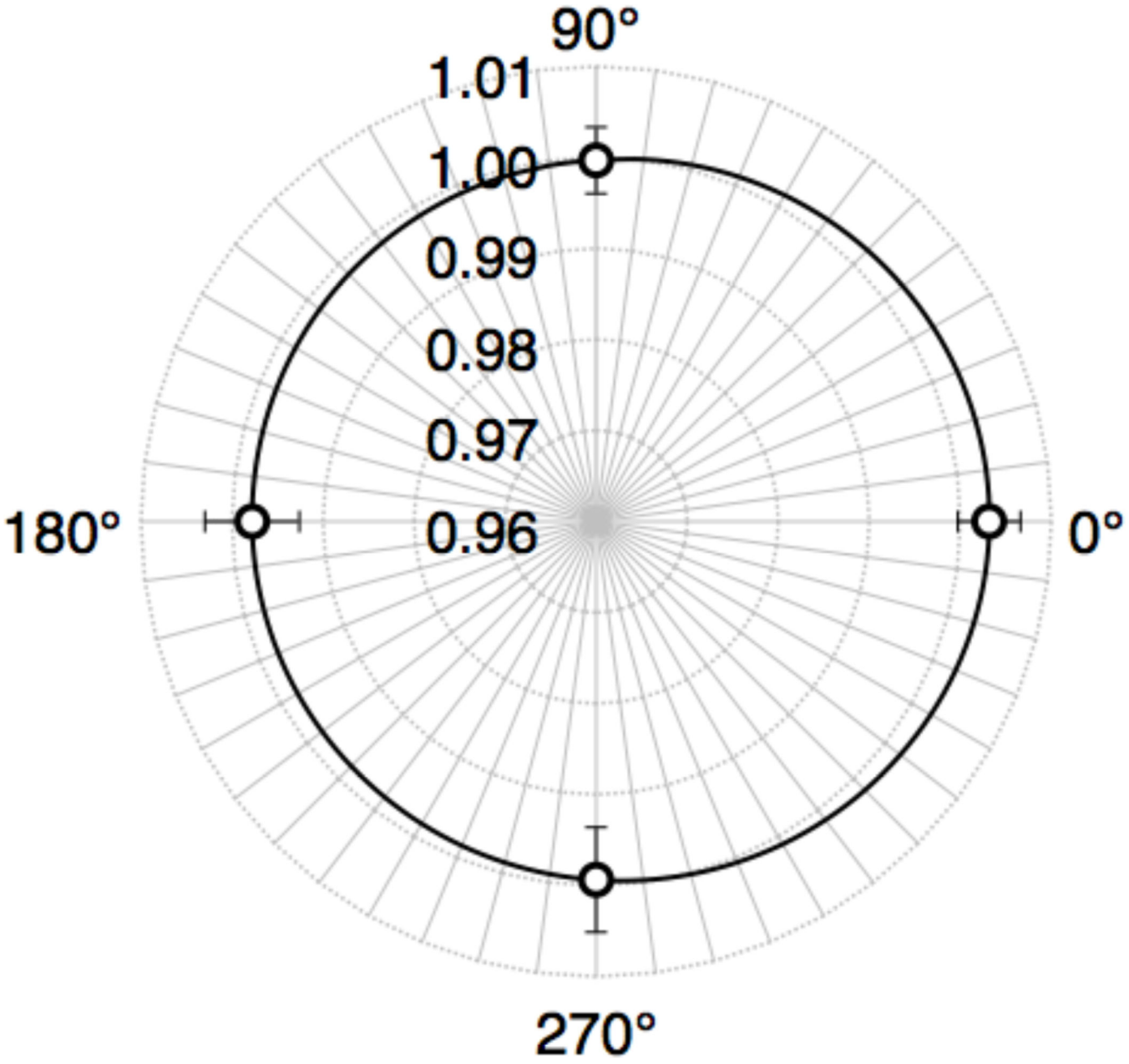

Figure 4.
The angular response of the real-time air ionization chamber. Air kerma values normalized to the average of the four angular measurements are plotted.

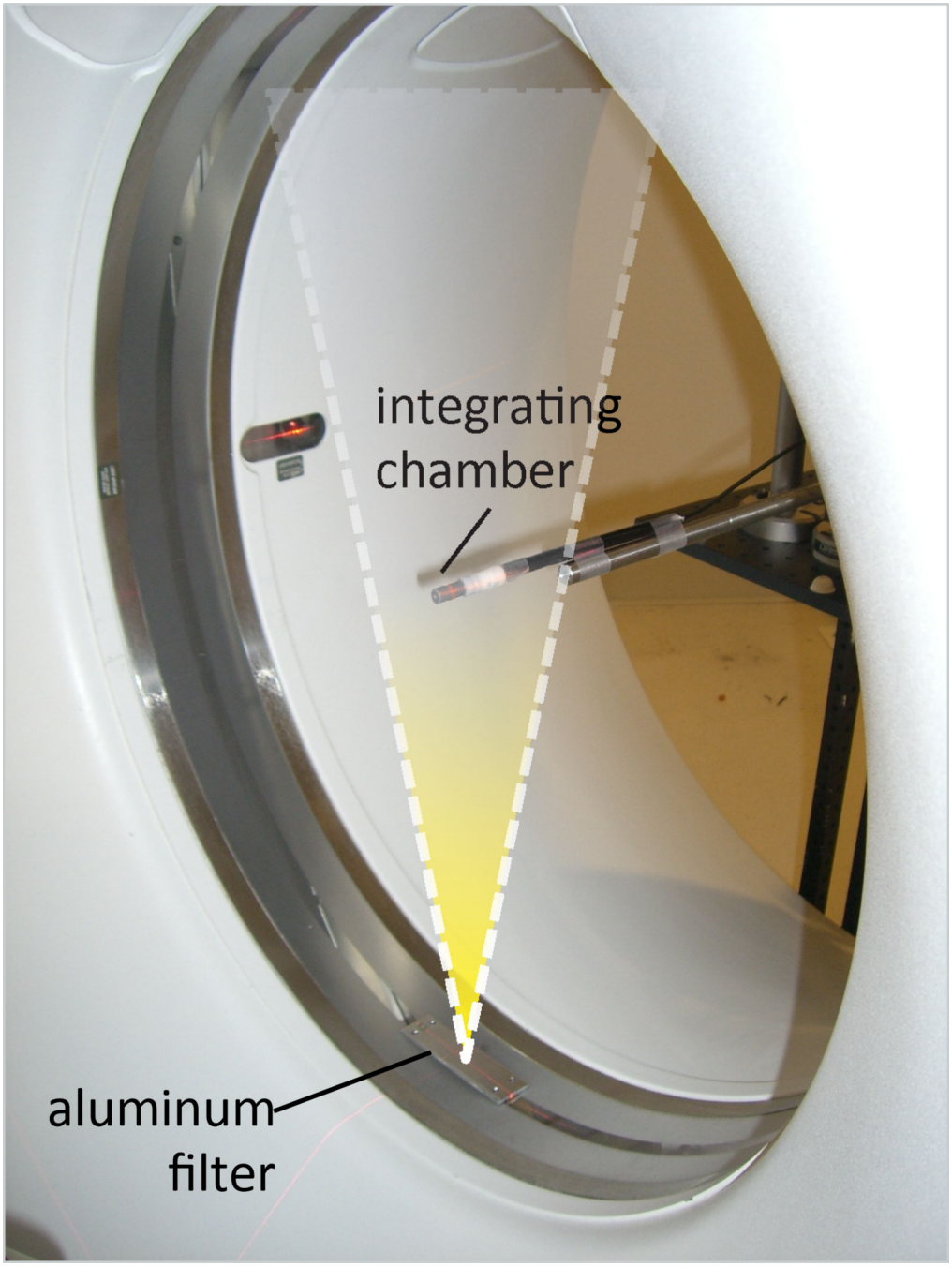

Figure 5.
Photograph of the system set up for the conventional HVL measurements. The aluminum filters from the AAF were removed and placed on the bottom of the CT gantry so that they attenuated the incident x-ray (held stationary at the 6 o'clock position). A 0.6 cc integrating air ionization chamber was placed at the laser-indicated isocenter.

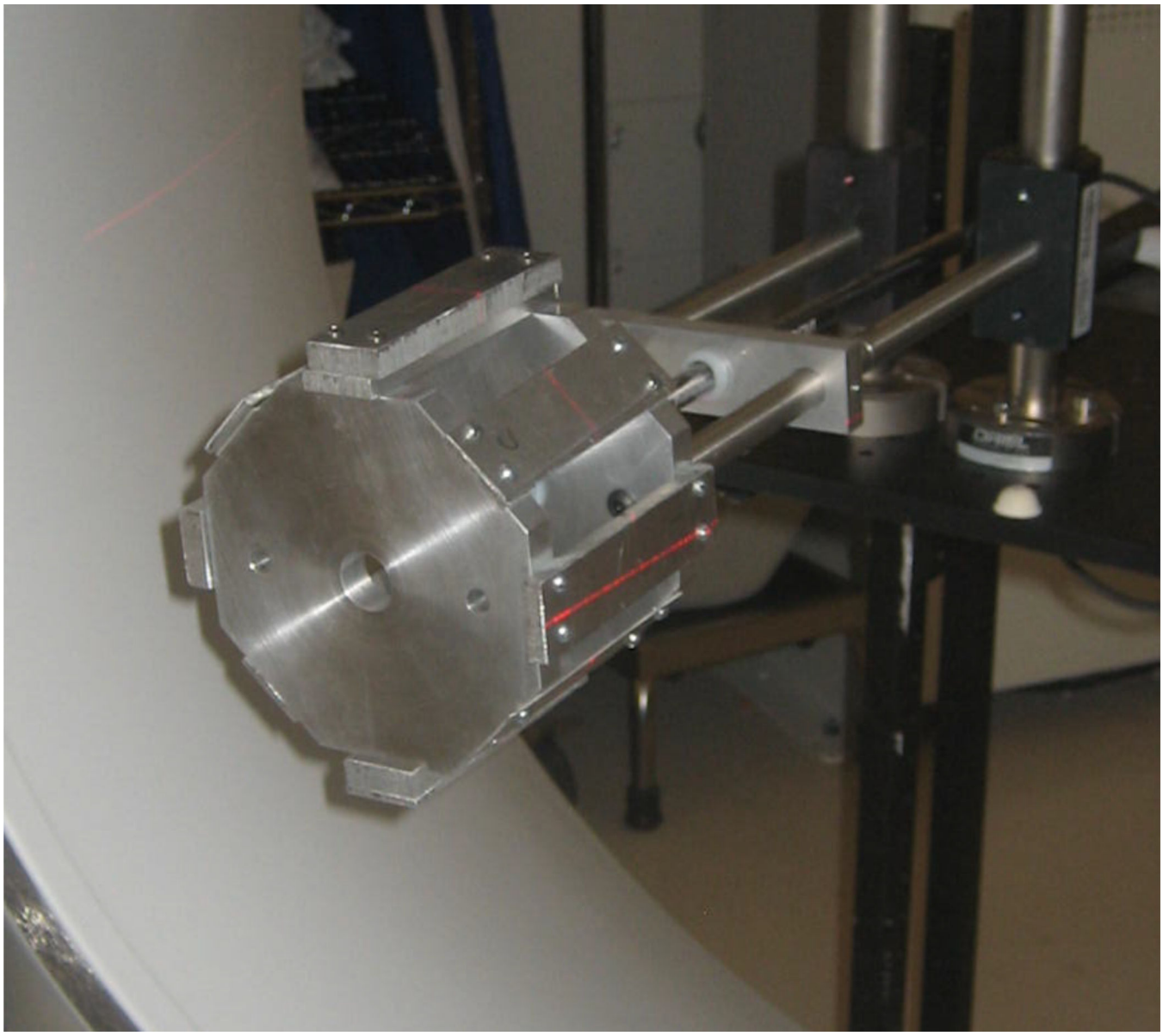

Figure 6.

Photograph of the AAF_{small} extended in the gantry of the CT scanner for measurements using a rotating source. The real-time dose probe, hidden by the endplate in this photo, was centered within the apparatus at isocenter.

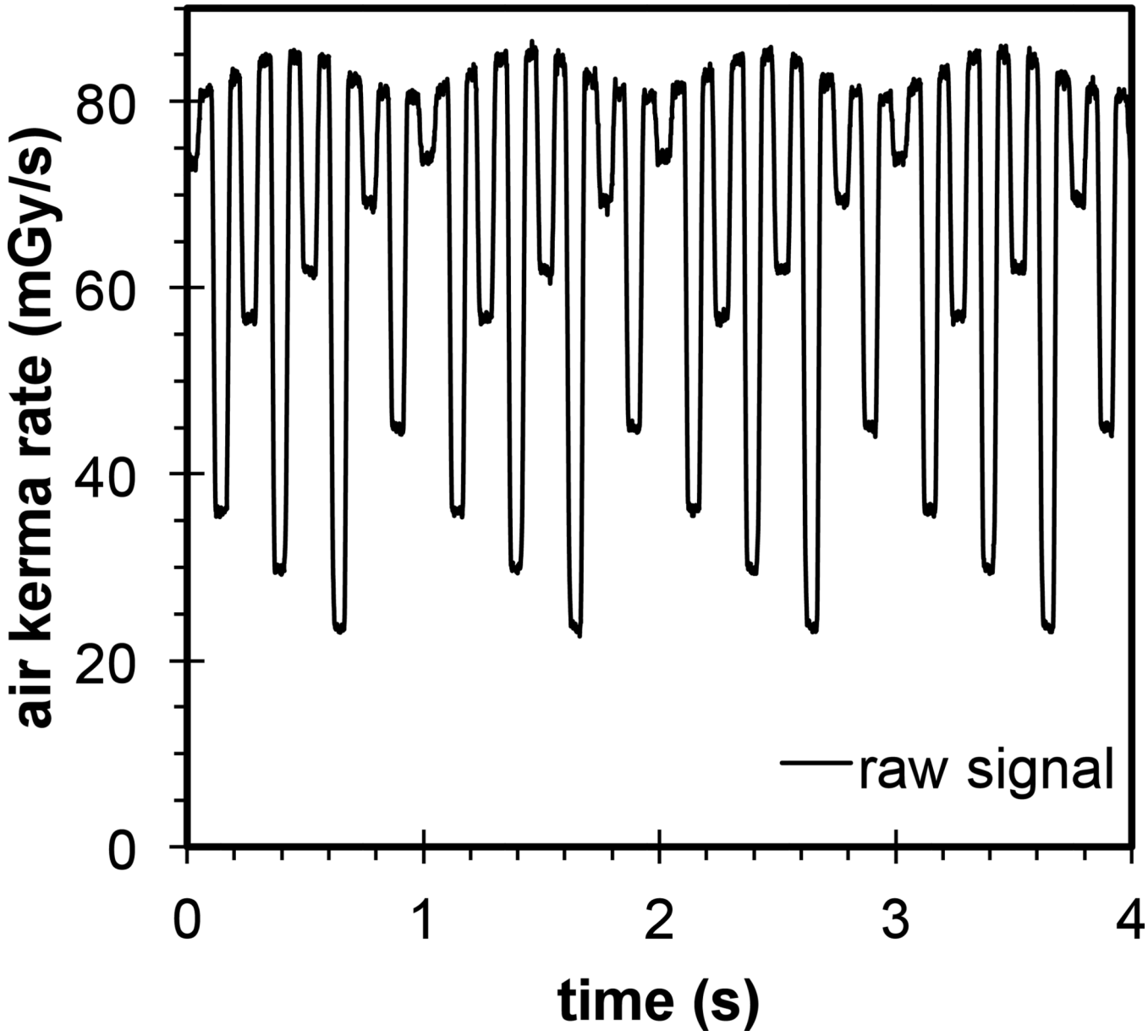

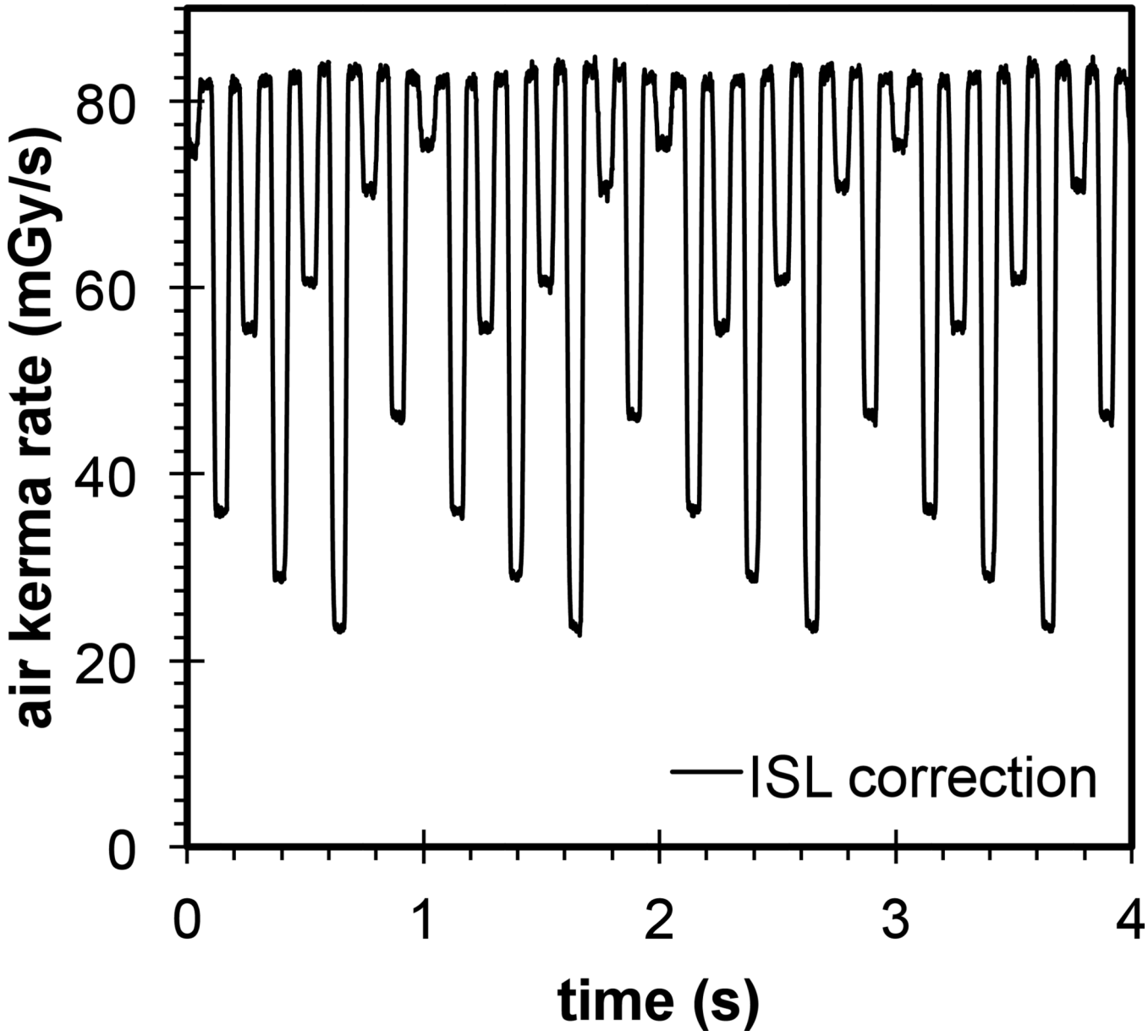

Figure 7.

Plot of (a) the raw signal acquired with the real-time air ionization (RTAI) chamber and (b) the signal when corrected for the inverse square law. The signal was acquired using a standard abdomen/pelvis protocol on a clinical CT scanner with the AAF_{small}.

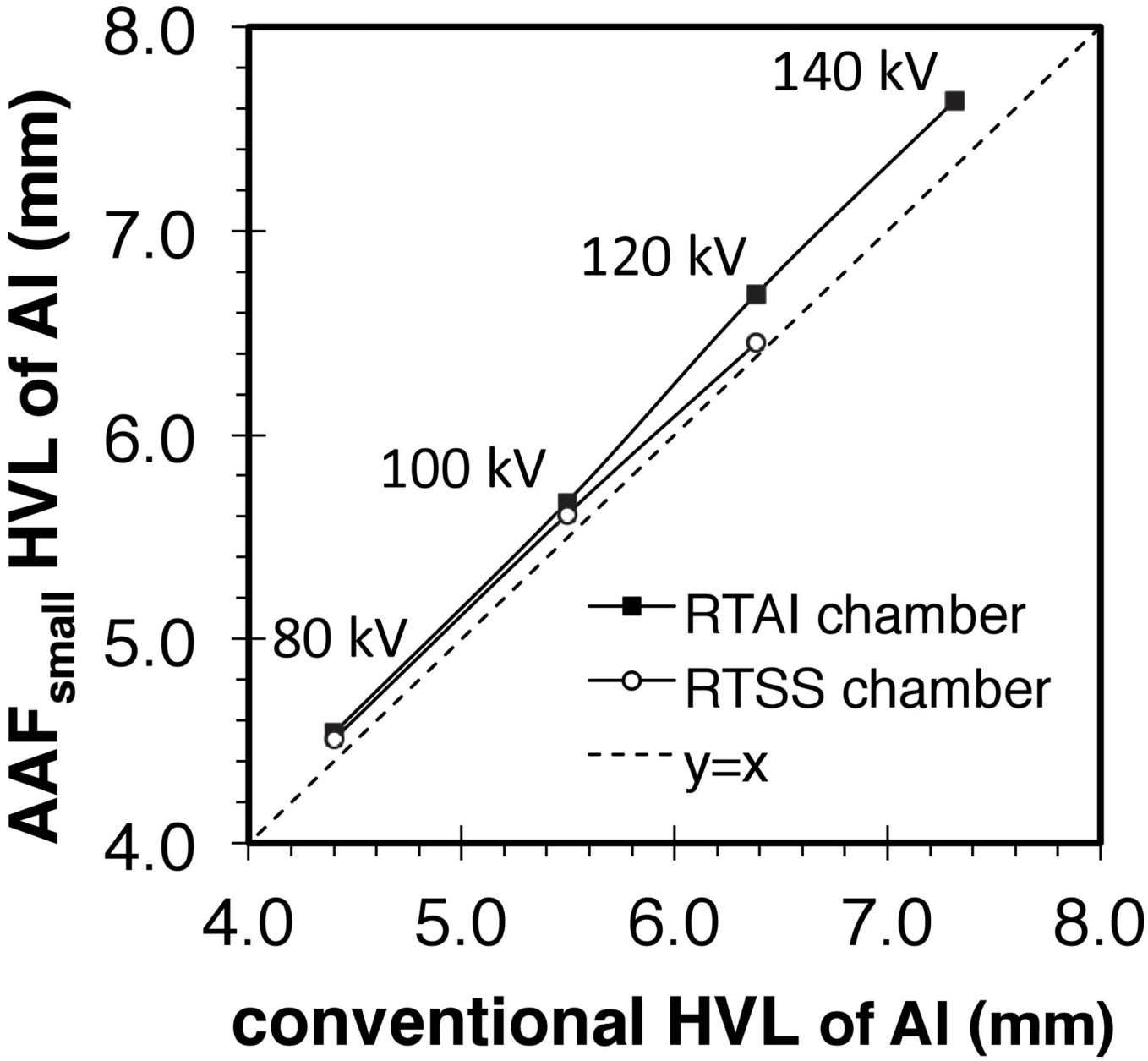

Figure 8.
Comparison of HVL measurements made with the AFF_{small} with conventional HVL values while varying tube potential (medium bow tie filter in service mode).

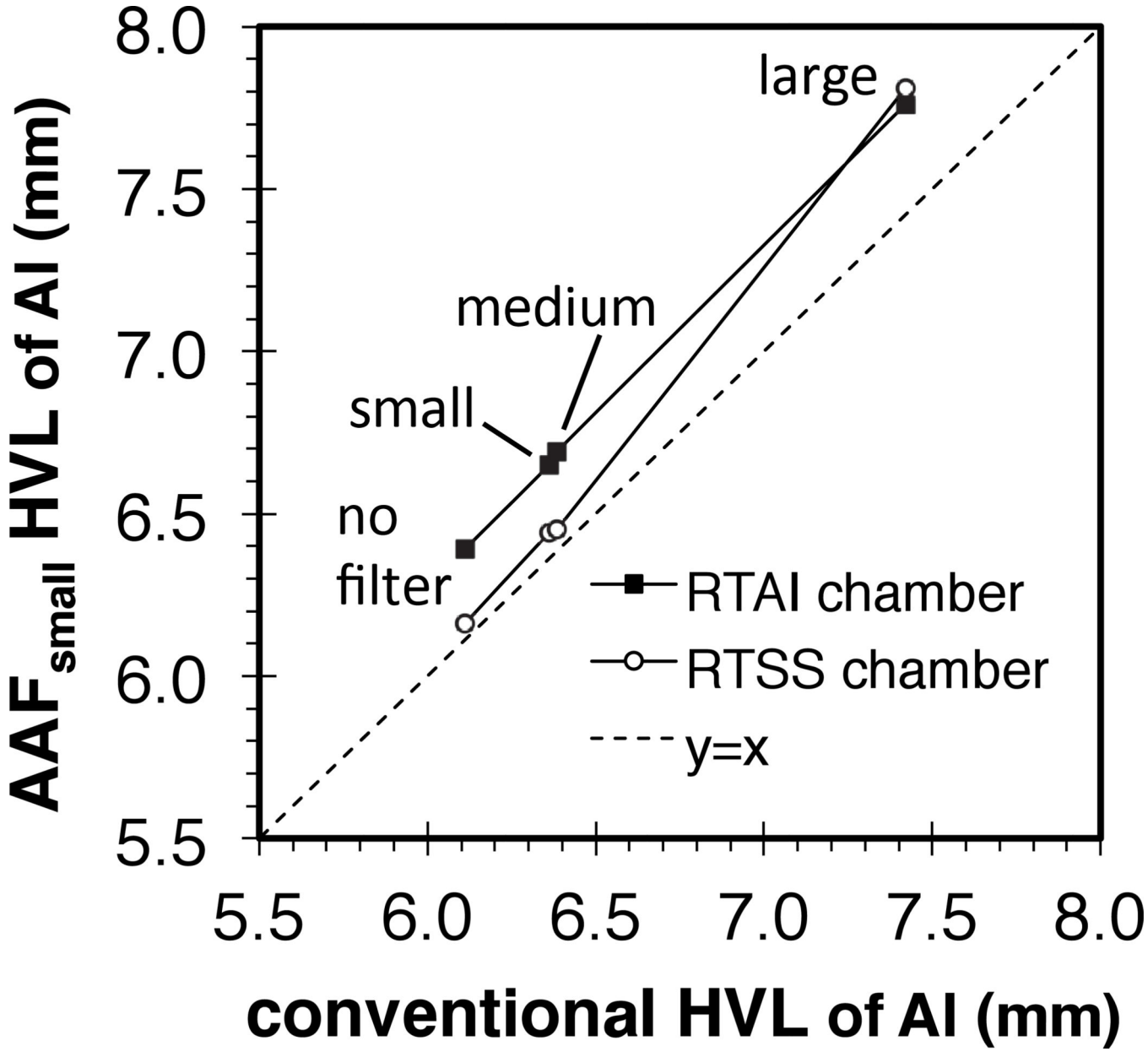

Figure 9.
Comparison of HVL measurements made with the AFF_{small} with conventional HVL values while varying bow tie filters (120 kV in service mode).

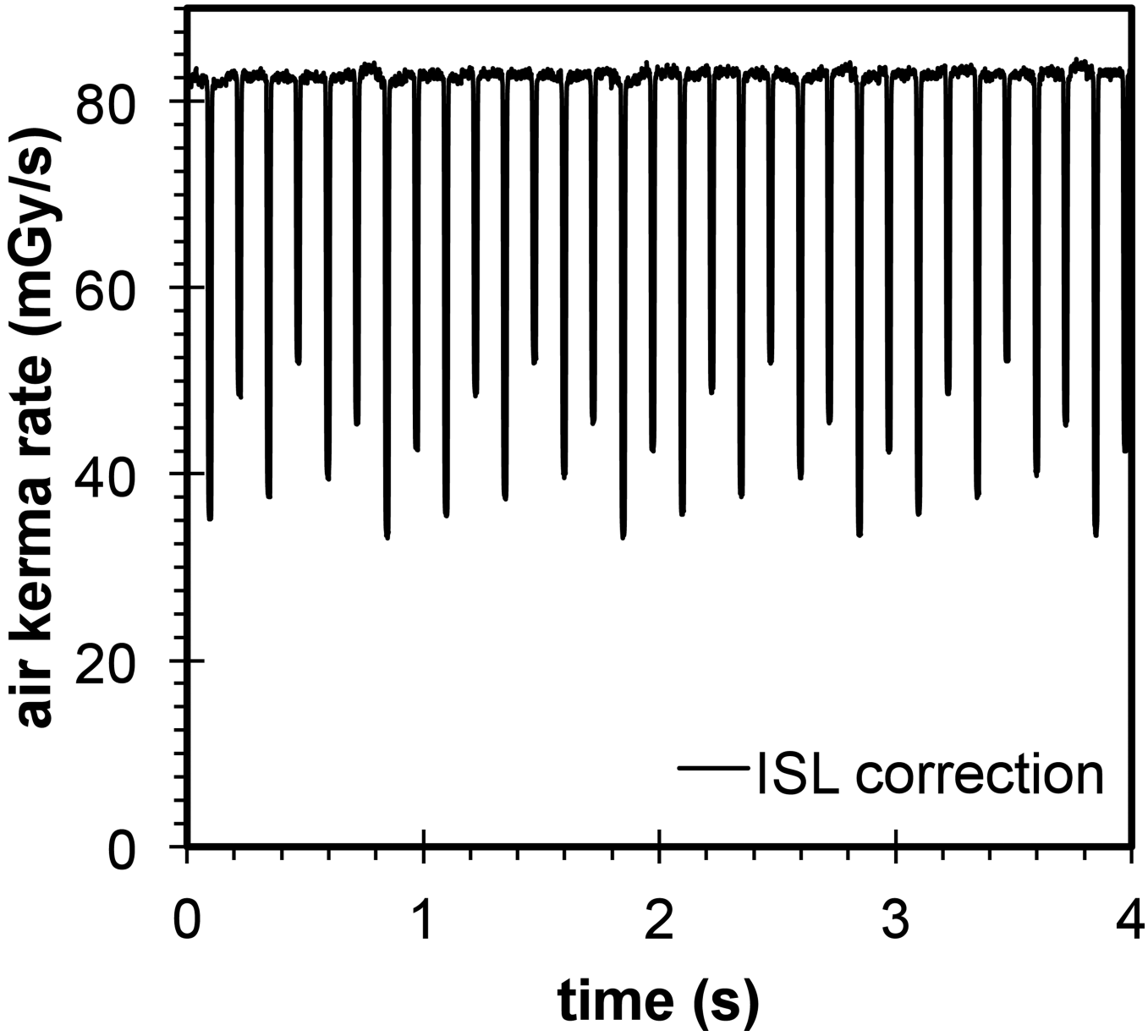

Figure 10.
Plot of the ISL corrected signal obtained when using the AAF_{large}. The signal was acquired with a standard abdomen/pelvis protocol at 120 kV with a large bow tie filter.

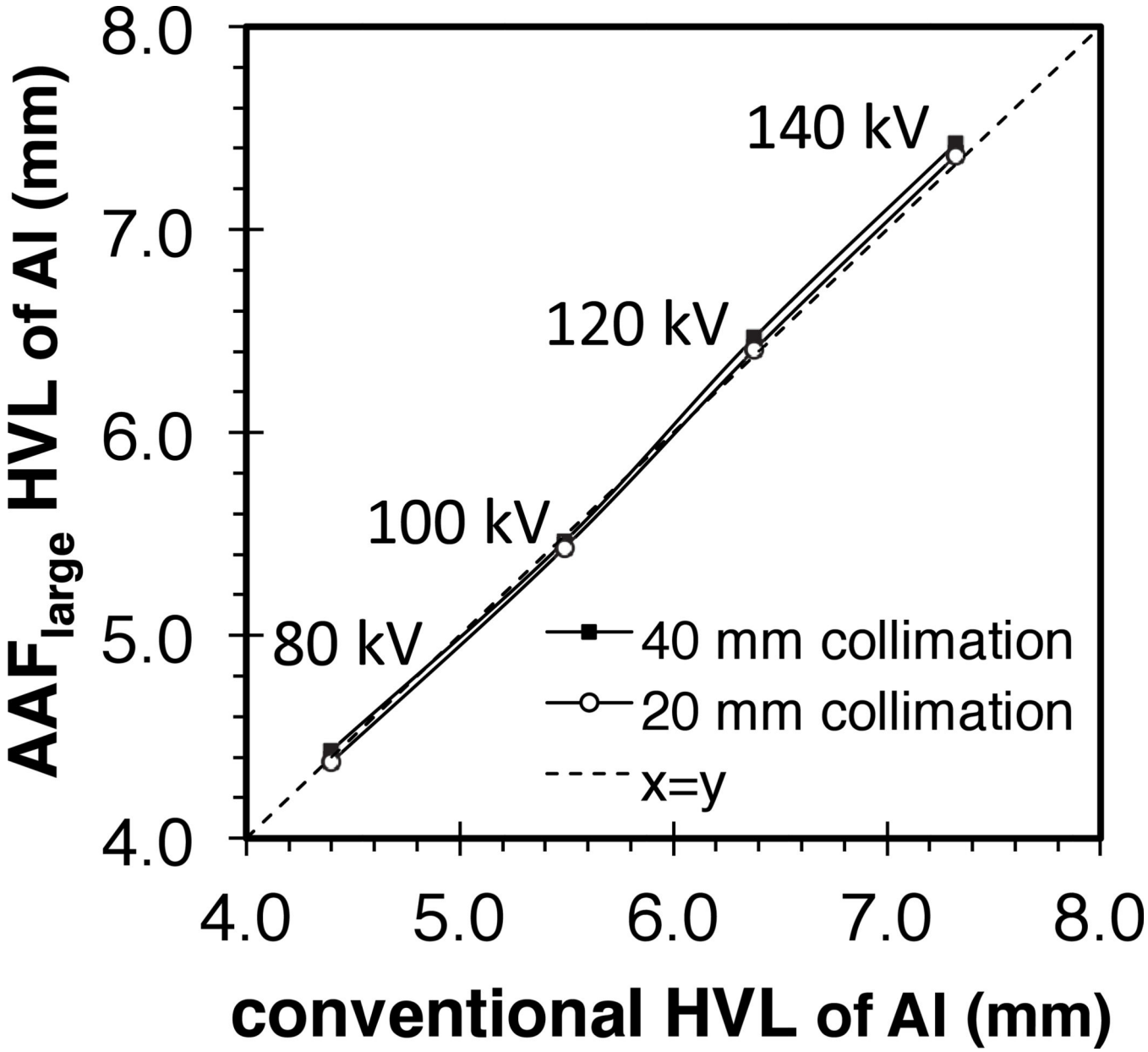

Figure 11.

Results from HVL measurements using the AAF_{large} as a comparison plot. The HVL was measured on the clinical CT scanner using a medium bow tie filter across different tube potentials with the abdomen/pelvis protocol.

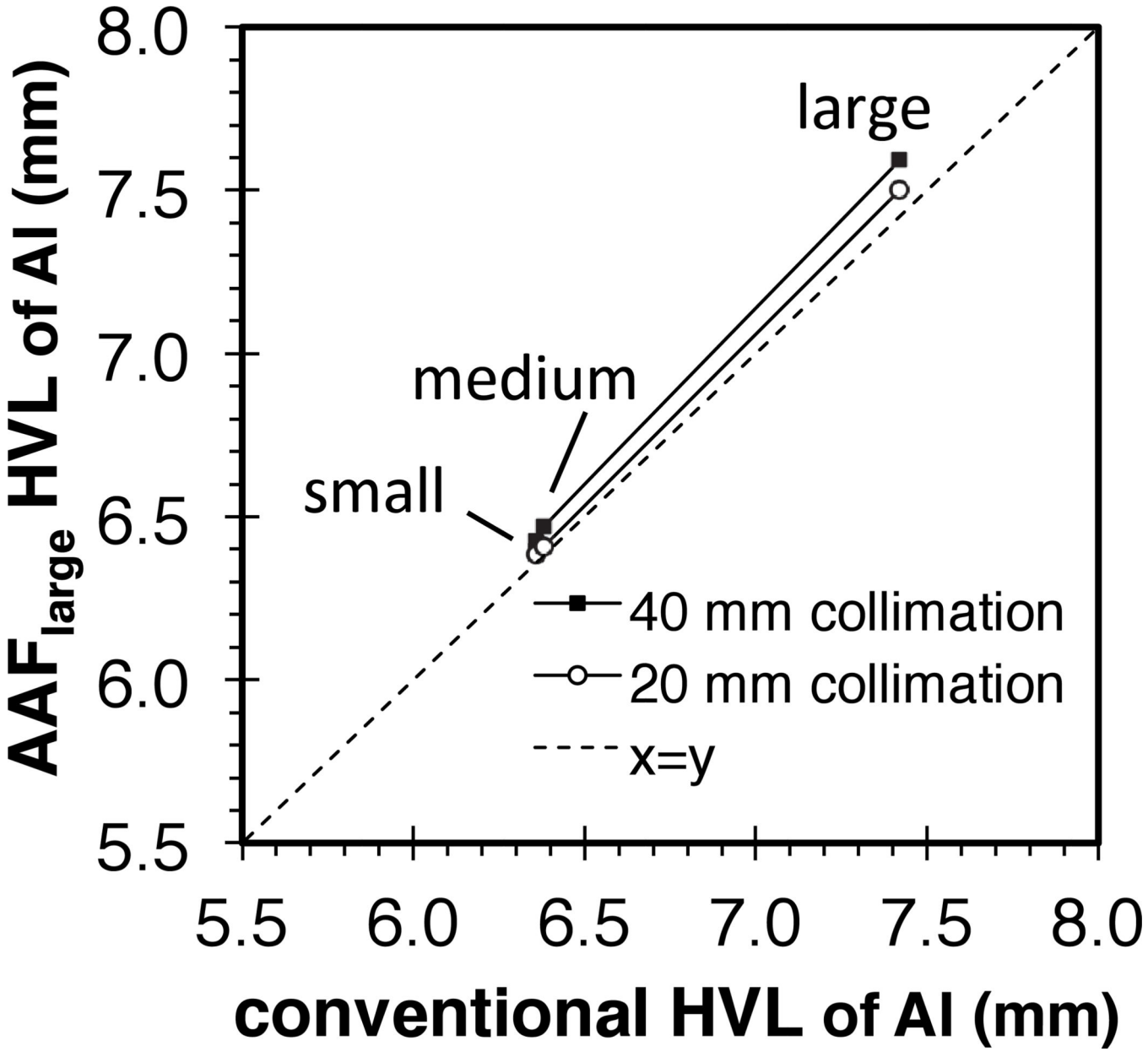

Figure 12.

Results from HVL measurements using the AAF_{large} as a comparison plot. The HVL was measured using different bow tie filters at 120 kV with a routine abdomen/pelvis protocol.

Table 1

HVL measurements on the clinical CT scanner made using three different methods. The conventional method, with a stationary source, was used as the reference method (3rd column). A paired t-test was performed between the HVL measurements obtained conventionally and with the AAF configuration (bottom row). The AAF_{small}, with a diameter of 122 mm, using a rotating source with helical mode and a real-time dose probe (4th and 6th columns), was found to agree with the conventional measurements of HVL with an average relative difference of 3.2%. The AAF_{large}, with a diameter of 505 mm, decreased the relative difference to 0.6%.

			AAF_{small} (service mode, collimated to active volume)				AAF_{large} (clinical mode, RTAI chamber)			
tube potential [kV]	**bow tie filter**	**Conventional method [mm]**	**RTAI chamber [mm]**	**relative difference [%]**	**RTSS chamber [mm]**	**relative difference [%]**	**20 mm beam width [mm]**	**relative difference [%]**	**40 mm beam width [mm]**	**relative difference [%]**
80	Air		4.32		4.29					
	Small		4.52		4.46		4.35		4.37	
	Medium	4.4	4.54	3.15	4.51	2.47	4.37	0.60	4.43	0.75
	Large		5.4		6.27		5.24		5.29	
100	Air		5.41		5.26					
	Small		5.63		5.54		5.40		5.44	
	Medium	5.49	5.67	3.19	5.61	2.1	5.43	1.07	5.46	0.50
	Large		6.68		6.78		6.45		6.50	
120	Air	6.11	6.39	4.59	6.16	0.82				
	Small	6.36	6.65	4.54	6.44	1.24	6.38	0.36	6.42	1.00
	Medium	6.38	6.69	4.80	6.45	1.04	6.41	0.43	6.47	1.39
	Large	7.42	7.76	4.58	7.81	5.25	7.50	1.09	7.59	2.32
140	Air		7.32		7.01					
	Small		7.72		7.24		7.32		7.35	
	Medium	7.32	7.64	4.42	*a*		7.36	0.59	7.42	1.39
	Large		8.74		8.7		8.49		8.59	
				$p < 0.001$		$p = 0.05$		$p > 0.5$		$p = 0.05$

[a] Measurement not collected due to user error